Theor Chem Acc (2010) 127:573–585
DOI 10.1007/s00214-010-0751-5

REGULAR ARTICLE

Computation of some thermodynamics, transport, structural properties, and new equation of state for fluid neon using a new intermolecular potential from molecular dynamics simulation

Mohsen Abbaspour · Elaheh K. Goharshadi

Received: 11 January 2010 / Accepted: 24 March 2010 / Published online: 8 June 2010

Abstract A new pair potential energy function of neon has been determined via the inversion of reduced viscosity collision integrals at zero pressure and fitted to obtain an analytical potential form. The pair potential reproduces the second virial coefficient, viscosity, thermal conductivity, and self-diffusion coefficient of neon in a good accordance with experimental data over wide ranges of temperature and density. We have also performed molecular dynamics simulation to obtain some thermodynamics, transport, and structural properties of fluid neon at different temperatures and densities using our calculated pair potential supplemented by quantum corrections following the Feynman–Hibbs approach. The significance of this work is that the three-body expression of Wang and Sadus (J Chem Phys 125:144509–1, 2006) can be used to improve the prediction of the pressures of neon without requiring an expensive three-body calculation. The molecular dynamics simulation of neon has been also used to determine a new equation of state for neon. Our results are in a good agreement with experiment and literature values.

Keywords Inversion method · Potential energy function · Second virial coefficient · Viscosity · Thermal conductivity · Self-diffusion coefficient · Molecular dynamics simulation · Quantum corrections · Feynman–Hibbs approach · Three-body interactions · Equation of state

M. Abbaspour (✉)
Department of Chemistry, Sabzevar Tarbiat Moallem University, Sabzevar, Iran
e-mail: abbaspour@sttu.ac.ir

E. K. Goharshadi
Department of Chemistry, Ferdowsi University of Mashhad, 91779 Mashhad, Iran

1 Introduction

Molecular interactions are the key to understanding the structure and properties of liquids and solids and the properties of gases so it is not surprising that one observes increasing interest in the study of molecular interactions which are of so much importance in chemistry, physics, and biology.

Intermolecular pair potential can be obtained from both experimental observations and theoretical (such as ab initio) calculations. Two procedures have been used for extracting the intermolecular potential energy function from the experimental data. They are fitting and inversion methods. In a fitting procedure, a model potential is adopted with a certain number of adjustable parameters which are varied until a good fit is obtained to a given set of experimental data. The potentials obtained from this method do not appear to be unique since they depend upon the range of temperature employed and the property chosen for the test. The aim of an inversion method is to obtain the potential by considering the experimental data as a functional instead of fitting the data to a constrained potential form having a few parameters [1, 2].

While neon does not display dramatic quantum effects of helium, these effects cannot be ignored and the neglect of quantum effects can be a source of irreducible discrepancy when the experimental data and classical simulation results are compared [3, 4].

Two approaches have been proposed to consider the quantum effects, the so-called Wigner–Kirkwood (WK) and Feynman–Hibbs (FH) potentials. The WK potential arises from an expansion in powers of $\hbar$ of the partition function [5, 6] which has been used in the literature to estimate the quantum corrections on different properties [7].

The FH potential is obtained from the Feynman–Hibbs variational estimate of the quantum partition function [8], used in the present work, leads to a pair potential depends on temperature and easy to implement in a standard molecular dynamics (MD) or Monte Carlo (MC) simulation code [3].

The FH potential has been studied by Sese [9, 10] to calculate the thermodynamic and structural properties of the LJ systems such as neon. Also, Tchouar et al. [3, 4] computed the thermodynamic, structural, and transport properties of neon system using LJ potential via the FH approach. Recently, Goharshadi et al. [11] computed the thermodynamic properties of helium using a Hartree–Fock dispersion (HFD)-like potential with the FH potential.

Besides the two-body interactions, it is also well known [12–14] that three-body interactions can make a small but significant contribution to the energy of fluids. To obtain a quantitative agreement with experiment, pair potentials must be used in conjunction with three-body interactions [15].

There are many contributions to three-body interactions but the evidences [16] indicated that the triple-dipole term of Axilrod and Teller [17] alone is an excellent approximation. Nonetheless, the need for three-body calculations in addition to pair calculations represents a considerable computational impediment [15].

Marcelli and Sadus [16] have reported good results for the prediction of the vapor–liquid equilibria of the pure substances argon, krypton, and xenon using accurate two-body potentials such as the Barker–Fisher–Watts (BFW) potential plus three-body contributions. They also showed that there is a simple and accurate relationship between the two-body and three-body interactions that allows us to obtain the three-body effect in a simulation without any additional computational cost [18]. Recently, Goharshadi and her co-workers [11, 19] used an Hartree–Fock dispersion (HFD)-like potential with this relation to simulate the thermodynamic properties of helium, argon, krypton, and xenon with good agreement with the experimental and other theoretical data.

Several MD and MC simulations involving different approaches using different potentials were performed. The recent calculations taking into account quantum effects [4–6, 20–23] and three-body interactions [24, 25] cover only some state points of the phase diagram and could not approach the properties accurately.

The first purpose of the present paper is to determine an accurate neon pair potential energy function by inversion of the reduced viscosity collision integrals at zero pressure. The second aim is to compute the second virial coefficient, viscosity, thermal conductivity, and self-diffusion coefficient of neon using the calculated pair potential at different temperatures and densities and compared with experimental data.

Finally, we have performed molecular dynamics simulation to obtain some thermodynamic (pressure and energy), transport (self-diffusion coefficient and shear viscosity), and structural (radial distribution function) properties of fluid neon at different temperatures and densities using our calculated pair potential which has been obtained with an inversion of viscosity data and the three-body expression of Wang and Sadus [18]. We have also considered the quantum corrections for both potentials. The molecular dynamics simulation of neon has been also used to determine a new equation of state for neon.

2 Theory

2.1 Transport properties

Molecular transport processes deal with the transfer or movement of a given property such as momentum, energy, and mass by molecular movement through a system which can be a fluid (gas or liquid) or a solid.

The transport properties of a dilute gas can be expressed in terms of a set of collision integrals, $\Omega^{(l,s)}(T)$, characterized by the value of l and s [26], for example the viscosity of a pure gas depends on the collision integral $\Omega^{(2,2)}(T)$:

$$\eta = 5/16(mkT/\pi)^{1/2}\frac{1}{\sigma^2\Omega^{(2,2)*}(T*)}f_\eta \tag{1}$$

where m and n represent the mass of the molecule and number density, respectively. k is Boltzmann constant, and f_η represents the higher-order corrections of first kinetic theory approximation to viscosity. T^* is reduced temperature, namely $T^* = kT/\varepsilon$ (ε is well depth of potential). The parameter of $\Omega^{(2,2)*}$ is the reduced collision integral which is defined in general as:

$$\Omega^{(l,s)*}(T^*) = \Omega^{(l,s)}(T)/\pi\sigma^2 \tag{2}$$

where $\pi\sigma^2$ is the collision integral for the rigid sphere of diameter σ, and $\Omega^{(l,s)}$ is collision integral.

The temperature-dependent collision integral $\Omega^{(2,2)}$ for pure gases is explicitly related to pair potential (two-body) energy function, $U_{2B}(r)$, through the classical mechanical triple integral [26]. All of the information about the intermolecular potential is therefore contained in the collision integrals:

$$\Omega^{(2,2)}(T) = \frac{1}{6(kT)^4}\int_0^\infty Q^{(2)}(E)e^{-E/kT}E^3dE \tag{3}$$

$$Q^{(2)}(E) = 3\pi \int_0^\infty b(1 - 2\cos^2 \chi)db \tag{4}$$

$$\chi(b, E) = \pi - 2b \int_{r_O}^\infty \left[1 - \frac{b^2}{r^2} - \frac{U_{2B}(r)}{E}\right]^{-1/2} \frac{dr}{r^2} \tag{5}$$

where E is the relative kinetic energy of a pair of colliding molecules, $Q^{(2)}(E)$ is a transport cross section, b is the impact parameter, χ is the scattering angle, and r_o is the classical distance of closest approach in a collision.

2.2 The theoretical basis of inversion method

This inversion method based on viscosity has been used to obtain the interaction potentials from the extended principle of corresponding states [27–29]. It has been proved that this principle is capable of correlating equilibrium and transport properties of the noble gases over a very wide temperature range with an accuracy comparable to the best measurements [27–30]. According to this principle, the reduced viscosity collision integral, $\Omega^{(2,2)^*}$, for a noble gas is defined as:

$$0 \le T^* \le 1.2$$

$$\Omega^{(2,2)^*} = 1.1943(C_6/T^*)^{1/3}\left[1 + a_1(T^*)^{1/3} + a_2(T^*)^{2/3} + a_3(T^*) + a_4(T^*)^{4/3} + a_5(T^*)^{5/3} + a_6(T^*)^2\right] \tag{6}$$

$$1.2 \le T^* \le 10$$

$$\Omega^{(2,2)*} = \exp[0.46641 - 0.56991(\ln T^*) + 0.19591(\ln T^*)^2 - 0.03879(\ln T^*)^3 + 0.00259(\ln T^*)^4] \tag{7}$$

$$T^* \ge 10$$

$$\Omega^{(2,2)*} = (\rho^*)^2\alpha^2\left[1.04 + a_1(\ln T^*)^{-1} + a_2(\ln T^*)^{-2} + a_3(\ln T^*)^{-3} + a_4(\ln T^*)^{-4}\right] \tag{8}$$

where the values of C_6, α, ρ^*, V_o^*, and a_1 to a_6 are given in Refs. [28, 30].

The direct inversion procedure for the viscosity is based on idea that at a given T^*, the value of $\Omega^{(2,2)^*}$ is determined by the potential over only a small range of separation distance around a value of r [31]. It is possible to make this idea exact by defining a function G_η such that

$$U_{2B}(r) = G_\eta(T^*) \cdot T^* \tag{9}$$

and $\Omega^{(2,2)^*}$ is approximately defined by

$$\Omega^{(2,2)*} = (r/\sigma)^2 \tag{10}$$

where G_η is known as the inversion function. The values of G_η are given in Ref. [31].

In order to develop an iterative scheme, it is necessary to extrapolate potential, $U_{2B}(r)$ to both large and smaller separations. We have used a reasonable choice i.e., Lennard–Jones 12–6 function for the attraction and repulsion parts. In any event, it has been found that whatever forms of realistic extrapolation employed, the final potential obtained is essentially independent of the extrapolations employed [1]. At long range, this extrapolation performed by means of an inverse sixth-power function:

$$U_{2B}(r) = -C_6 r^{-6} \tag{11}$$

at short range by means of an inverse twelfth-power function:

$$U_{2B}(r) = Ar^{-12} \tag{12}$$

where $U_{2B}(r)$ is intermolecular pair potential function, r is the intermolecular separation, C_6 and A are constants.

The potential energy U_{2B}/ε can be obtained using Eq. 9 and the corresponding value of r/σ can be obtained using the collision integral calculated from Eq. 10. This process may be repeated until convergence is obtained. At each stage in the iteration process, the percent deviation of $\Omega^{(2,2)^*}(T^*)$ calculated from the potential and the corresponding-state values is determined.

Despite the considerable practical success of this inversion procedure, there has been no complete explanation of its mode of operation. The puzzle of very existence of the inversion procedure is compounded by two peculiar features of the process that are essential for its success. The first feature is the near, but not complete, universality of the inversion function, $G(T^*)$, among a whole class of potential functions possessing repulsive and attractive branches joined by a single minimum. The other remarkable feature of the inversion procedure is that it identifies a point on the experimental $\Omega^{(2,2)^*}$ versus temperature curve corresponding with a single point on the $U(r)$ function.

The preliminary attempt to explain these two features of the inversion procedure and hence the entire scheme has been made and is based upon a number of mathematical approximations of the various integrals linking the collision integral at a particular temperature to the potential [1].

3 Results and discussion

3.1 Intermolecular potential and collision integrals

The inner part of the potential can be obtained using the inversion method.

In other words, the inversion method cannot produce the pair potential function in the whole range of separations.

The second virial coefficient is more sensitive to the potential than the transport properties. The width of the

potential energy function may be defined in terms of the second virial coefficient for $T < \varepsilon/k$ [31]. Knowing the inner branch of the potential well from the viscosity in conjunction with the second virial coefficient helps us to determine the outer branch of the potential. The equations used for this purpose are as follows:

$$U_{2B}/\varepsilon = T^* - 1 \tag{13}$$

$$r_R^3 - r_L^3 = -(B - B_{\mathrm{HS}})N(T^*) \tag{14}$$

where r_R and r_L are the coordinates of the outer and inner wall of the potential well, respectively. B_{HS} is the second virial coefficient of a hard sphere, namely: $2\pi N_A\sigma^3/3$. The values of $N(T^*)$ have been given in Ref. [31]. The second virial coefficient, B, has been computed using the extended principle of corresponding states formula [30].

The pair potential energy function of neon has been obtained using the inversion of the reduced viscosity collision integrals at zero pressure. At long range, only the well width of the potential obtained from the second virial coefficient data is available. This has been used in conjunction with the inner part of the potential calculated using thew inversion method to obtain the potential energy in the whole separation range (Fig. 1).

We have compared our reduced calculated pair potential with the Aziz HDFC2 potential [32], an ab initio potential [20] with an 14s10p4d1f basis set applying fourth-order Moller–Plesset perturbation theory (MP4), and the Lennard–Jones (LJ) potential [33] in Fig. 1.

As Fig. 1 shows there is a better accordance between our calculated pair potential and the Aziz HDFC2 potential than the ab initio and LJ potentials which have shallower potential well. Our pair potential also shows good agreement with the ab initio potentials of Nasrabad et al. [24] and Leonhard and Deiters [25] in Fig. 1.

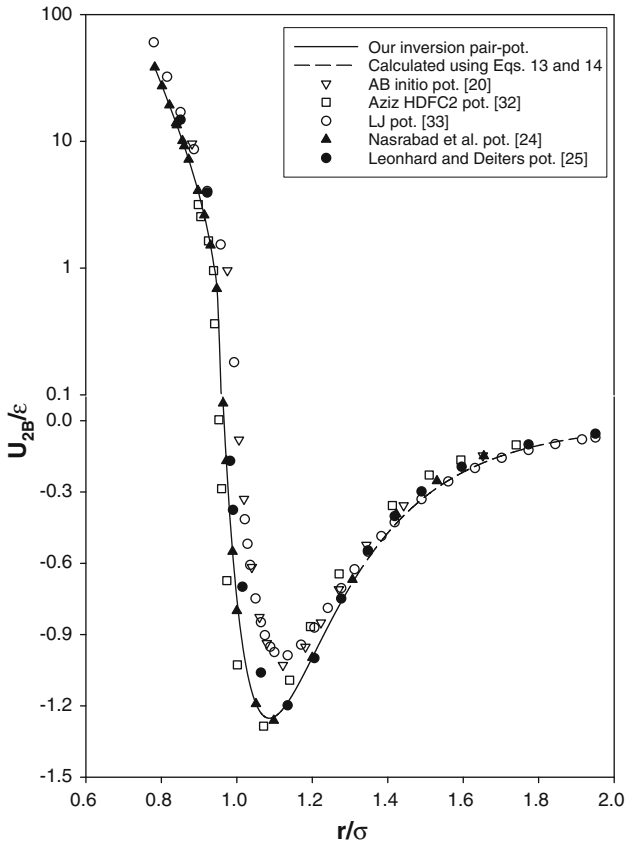

Fig. 1 Comparison between our potential energy function of neon calculated using inversion of reduced viscosity collision integrals at zero pressure and different literature potentials

Table 1 Dimensionless collision integrals $\Omega^{(l,s)*}$ and the related ratios[a] for neon at zero pressure

Log T^*	$\Omega^{(1,1)*}$	$\Omega^{(1,2)*}$	$\Omega^{(2,2)*}$	$\Omega^{(1,3)*}$	B^*	C^*
−1.0	5.6147	3.7846	6.5335	2.9607	1.2609	0.6740
−0.9	4.5110	3.1284	5.2283	2.5190	1.2339	0.6935
−0.8	3.6810	2.6472	4.2627	2.2038	1.2010	0.7191
−0.7	3.0633	2.2979	3.5489	1.9757	1.1708	0.7501
−0.6	2.6068	2.0413	3.0242	1.8003	1.1529	0.7831
−0.5	2.2678	1.8440	2.6381	1.6519	1.1519	0.8131
−0.4	2.0097	1.6807	2.3466	1.5155	1.1651	0.8363
−0.3	1.8046	1.5362	2.1125	1.3865	1.1831	0.8512
−0.2	1.6333	1.4040	1.9101	1.2666	1.1960	0.8596
−0.1	1.4847	1.2835	1.7264	1.1597	1.1980	0.8645
0.0	1.3539	1.1765	1.5589	1.0683	1.1889	0.8690
0.1	1.2390	1.0843	1.4100	0.9924	1.1721	0.8751
0.2	1.1397	1.0068	1.2824	0.9302	1.1524	0.8834
0.3	1.0549	0.9425	1.1766	0.8790	1.1341	0.8934
0.4	0.9835	0.8890	1.0908	0.8359	1.1197	0.9039
0.5	0.9235	0.8439	1.0218	0.7985	1.1104	0.9138
0.6	0.8727	0.8046	0.9663	0.7645	1.1060	0.9221
0.7	0.8288	0.7694	0.9207	0.7326	1.1057	0.9280
0.8	0.7899	0.7366	0.8820	0.7020	1.1075	0.9325
0.9	0.7546	0.7055	0.8474	0.6725	1.1097	0.9349
1.0	0.7218	0.6758	0.8149	0.6444	1.1106	0.9363
1.1	0.6909	0.6476	0.7831	0.6180	1.1090	0.9373
1.2	0.6619	0.6214	0.7511	0.5941	1.1036	0.9387
1.3	0.6350	0.5976	0.7188	0.5734	1.0935	0.9411
1.4	0.6105	0.5770	0.6864	0.5567	1.0787	0.9452
1.5	0.5889	0.5602	0.6547	0.5441	1.0608	0.9512
1.6	0.5709	0.5473	0.6251	0.5354	1.0420	0.9588
1.7	0.5564	0.5382	0.5989	0.5302	1.0250	0.9672
1.8	0.5456	0.5323	0.5772	0.5275	1.0112	0.9757
1.9	0.5380	0.5290	0.5603	0.5266	1.0013	0.9834
2.0	0.5331	0.5277	0.5481	0.5270	0.9950	0.9899

[a] $B^* = [5\Omega^{(1,2)*} - 4\Omega^{(1,3)*}]/\Omega^{(1,1)*}$ and $C^* = \Omega^{(1,2)*}/\Omega^{(1,1)*}$

We have also calculated the most commonly needed collision integrals and their ratios for neon at zero pressure in Table 1. These quantities are needed for computation of the transport properties at any temperature and pressure.

3.2 Second virial coefficient

The reduced second virial coefficient $B^* = B(T)\Big/\frac{2\pi N_A \sigma^3}{3}$ for neon is computed using the classical formula:

$$B(T) = 2\pi N_A \int_0^\infty \left[1 - e^{-U_{2B}(r)/kT}\right] r^2 dr \tag{15}$$

It should be noted that we have reduced all of the results and literature values using the LJ parameters for neon ($\varepsilon/k = 32.8$ K, $\sigma = 2.82$ Å) [33].

The calculation of the second virial coefficient can be considered as a critical test for a potential [1]. The agreement between our calculated values of second virial coefficient and the experimental data [34] in Fig. 2 is better than other literature values calculated using ab initio and Aziz potentials and this confirms the validity of our potential.

3.3 Calculation of transport properties

3.3.1 Viscosity

In the 1980s, Rainwater and Friend [35, 36] developed a microscopically based theoretical model for the second transport virial coefficients of moderately dense gases. According to their model, viscosity, η, can be expanded as:

$$\eta = \eta_0(1 + B_\eta \rho + \ldots) \tag{16}$$

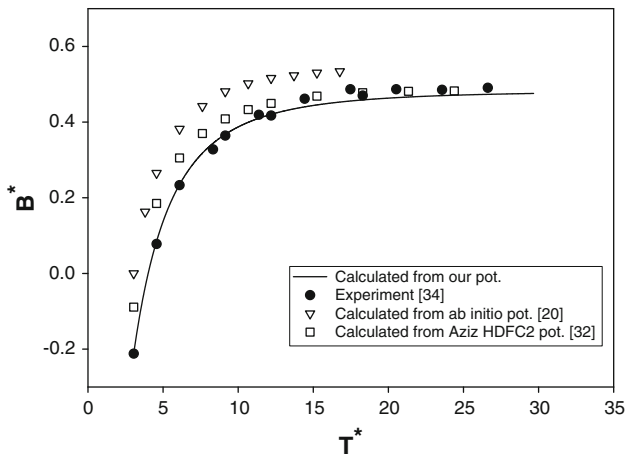

Fig. 2 Comparison between our calculated second virial coefficients using our potential and different literature potentials with the experimental values

where η_o is the limiting low density viscosity near zero density, ρ is the number density, and B_η is second viscosity virial coefficient. In this model, B_η is dependent on the intermolecular potential. Rainwater and Friend [35, 36] used the LJ (12–6) potential for the calculation of B_η.

In the Rainwater–Friend theory, which deals with more realistic potentials than LJ potential, the reduced second viscosity virial coefficient, B_η^*, is assumed to be the sum of three contributions:

$$B_\eta^* = B_\eta^{(2)*} + B_\eta^{(3)*} + B_\eta^{(M-D)*} \tag{17}$$

where $B_\eta^{(2)*}$ represents the contribution from the nonlocality of monomer–monomer collisions. $B_\eta^{(3)*}$ is the effect of the presence of a third particle during a monomer–monomer collision and $B_\eta^{(M-D)*}$ is the contribution from monomer–dimer collisions.

Although the Rainwater–Friend theory is the most comprehensive treatment of the transport coefficients for moderately dense gases, it is known that the LJ (12–6) potential is crude and should be replaced by more realistic potentials.

Najafi et al. [37] have calculated the second viscosity virial coefficient of some gases based on the Rainwater–Friend theory using the most accurate potentials available for the gases. Their results implied that there may be a universal function for calculation of B_η^*(the reduced second viscosity virial coefficient) for all gases at moderate pressure over a wide temperature range. According to this correlation [37], the viscosity of moderately dense gases (up to 2 mol dm^{-3}) at specified temperature can be calculated via the equation:

$$\eta = \eta_o\,(1 + N_A \sigma^3 B_\eta^* \rho) \tag{18}$$

where N_A is Avogadro's number and σ is the collision diameter. B_η^* is the universal function of $(T^*)^{-i}$ in the form of a sixth order polynomial:

$$B_\eta^* = \sum_{i=1}^{6} b_i (T^*)^{-i} \tag{19}$$

where T^* is the reduced temperature and b_i is the coefficient of the universal correlation function. The values of b_i for the gases are given in Ref. [37].

The reduced viscosity $\left(\eta^* = \frac{\eta\sigma^3}{\varepsilon\tau},\ \tau = \left(\frac{m\sigma^2}{\varepsilon}\right)^{1/2}\right)$ of neon at different temperatures and atmospheric pressure has been calculated using Eq. 18 and compared with the experimental values [38, 39] in Fig. 3.

3.3.2 Thermal conductivity

Like the viscosity, the thermal conductivity, λ, of moderately dense gases (up to 2 mol dm^{-3}) at a specified temperature and density can be calculated via the equation [37]:

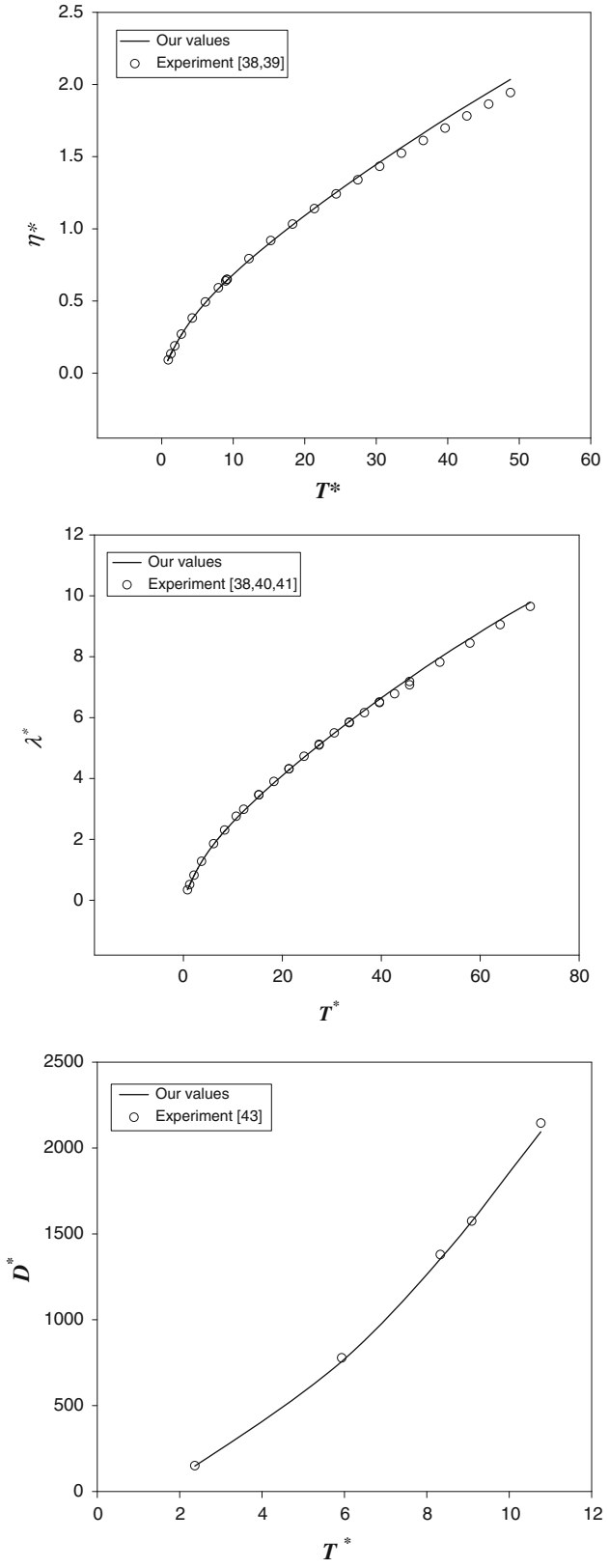

Fig. 3 Comparison between our calculated transport properties using our potential with the experimental values at atmospheric pressure

$$\lambda = \lambda_0(1 + N_A\sigma^3 B_\lambda^* \rho) \tag{20}$$

where λ_0 is the limiting low-density thermal conductivity near zero density which is density independent and B_λ^* is the reduced second thermal conductivity virial coefficient.

B_λ^* is dependent on the intermolecular potential and the temperature. Rainwater and Friend considered the reduced thermal conductivity virial, B_λ^*, to be made up of three contributions (such as B_η^*):

$$B_\lambda^* = B_\lambda^{(2)*} + B_\lambda^{(3)*} + B_\lambda^{(M-D)*} \tag{21}$$

As for B_η^*, the superscripts represent the contribution from the nonlocality of monomer–monomer collisions, the effect of the presence of a third particle during a monomer–monomer collision, and monomer–dimer collisions, respectively.

Najafi et al. [37] showed that there exists a corresponding states behavior for B_λ^* for all noble gases:

$$B_\lambda^* = a_o + \frac{a_1}{T^*} \tag{22}$$

The values of parameters a_o and a_1 have been given in Ref. [37].

The reduced thermal conductivity $\left(\lambda^* = \lambda\frac{\sigma^2}{k}\left(\frac{m}{\varepsilon}\right)^{1/2}\right)$ of neon at different temperatures and at atmospheric pressure has been calculated using Eq. 20 and compared with the experimental values [38, 40, 41] in Fig. 3.

3.3.3 Self-diffusion coefficient

According to the Enskog-Chapman theory [26, 42], the self-diffusion coefficient of moderately dense gases can be calculated by the equation:

$$D = \frac{3}{16}\left(\frac{kT}{m\pi}\right)^{1/2}\frac{1}{n\sigma^2\Omega^{(1,1)*}(T^*)}f_D \tag{23}$$

where f_D represents the higher-order correction to the first kinetic theory approximation.

The self-diffusion coefficient $\left(D^* = D\frac{\left(\frac{m}{\varepsilon}\right)^{1/2}}{\sigma}\right)$ of neon at different temperatures and atmospheric pressure has been calculated using Eq. 23 and compared with the experimental values [43] in Fig. 3.

We have summarized the results in Table 2. In this table, we have also presented our results of reduced viscosity and thermal conductivity of neon at different pressures.

3.4 Molecular dynamics simulation of neon

3.4.1 Intermolecular potential

In order to use our calculated pair potential in the MD simulation, we have fitted our reduced potential of neon

Table 2 Summary of the results of different properties calculated from our pair potential

Property	$(T^*_{min}$–$T^*_{max})$	$(P^*_{min}$–$P^*_{max})$	$(\%Dev_{min}$–$\%Dev_{max})$[a]
B^*	(4.57)–(29.67)	0.005	(0.55)–(10.92)
λ^*	(0.83)–(70.12)	0.005	(0.00)–(3.13)
	(9.11–9.46)	(0.071)–(1.780)	(1.33)–(2.46)
η^*	(0.91)–(48.78)	0.005	(0.17)–(4.70)
	(2.36–11.40)	(0.001)–(0.700)	(1.18)–(2.96)
D^*	(2.37)–(10.77)	0.005	(0.28)–(2.74)

[a] The absolute value has been considered

with a HFD-like potential like for other noble gases in our previous works [11, 19] to obtain an analytical potential form:

$$U^*_{2B}(x) = A^* \exp(-a^* x) - \frac{C^*_6}{x^6} - \frac{C^*_8}{x^8} - \frac{C^*_{10}}{x^{10}} \tag{24}$$

where $x = r/\sigma$ and $U^*_{2B} = U_{2B}/\varepsilon$ (σ is distance at which the intermolecular potential has zero value and ε is well depth of the potential). The values of the parameters of the potential of neon have been given in Table 3.

Wang and Sadus [18] showed that there is a simple and accurate relationship between the two-body (U_{2B}) and three-body (U_{3B}) potential energies of a fluid as:

$$U_{3B} = -\frac{0.85\upsilon\rho U_{2B}}{\varepsilon\sigma^6} \tag{25}$$

where υ is the nonadditive coefficient which is equal to 1.7047×10^{-109} Jm^9 [24]. $\rho = N/V$ is the number density, σ is the distance at which the intermolecular potential is zero.

The overall reduced interaction potential, two-body plus three-body, (U^*_T) is as follows:

$$U^*_T(x) = U^*_{2B}(x)\left[1 - \frac{0.85\upsilon\rho}{\varepsilon\sigma^6}\right] \tag{26}$$

The significance of this equation is that it allows us to use two-body potentials to predict accurately the properties of real fluids without incurring the computational cost of three-body calculations. In this work, we have used this equation in our simulations with the two-body potentials. We have also applied the correction formula proposed by Smit et al. [44] for calculating the configuration pressure when the total potential (two-body plus three-body interaction potential) is used.

Recently, Tchouar et al. [3] showed that the quantum corrections for neon system using the FH potential which has been obtained from quantum partition function (without exchange) for a canonical ensemble of atoms is superior than the WK potential and it is able to correct the discrepancy existing between the experiment and classical simulation both for the thermodynamical quantities and transport coefficients. Therefore, we have used the FH potential with both reduced two-body and total potentials (U^*_{Q2B} and U^*_{QT}):

$$U^*_{Q2B}(x) = U^*_{2B}(x) + \frac{T^*\hbar^2\sqrt{\frac{m}{\varepsilon}}}{24\mu\sigma}\left[U^{*\prime\prime}_{2B}(x) + 2\frac{U^{*\prime}_{2B}(x)}{x}\right] \tag{27}$$

$$U^*_{QT}(x) = U^*_{T}(x) + \frac{T^*\hbar^2\sqrt{\frac{m}{\varepsilon}}}{24\mu\sigma}\left[U^{*\prime\prime}_{T}(x) + 2\frac{U^{*\prime}_{T}(x)}{x}\right] \tag{28}$$

where μ is the reduced mass and $\hbar = h/2\pi$ (h is the Planck's constant). The prime and the double prime are the first and second x derivatives, respectively. As Eqs. 27 and 28 show, the Feynman–Hibbs quantum correction terms depend on mass and temperature.

Table 3 The coefficients of our pair potential of neon, Eq. 24

Coefficient	Value
ε/k (K)	42.2500
σ (Å)	2.7590
A^*	20341.90000
a^*	10.3929
c^*_6	1.2839
c^*_8	7.8407
c^*_{10}	−8.2396

3.4.2 Simulation details

The MD simulations using MOLDY software [45] have been performed for a system of 1,000 atoms in a cubic box, and the conventional periodic boundary condition has been applied. We have used the NVT ensemble using a Nosé-Hoover thermostat for atoms interacting via the reduced two-body potential, U^*_{2B}, (Eq. 24), reduced quantum two-body potential, U^*_{Q2B}, (Eqs. 24 and 27), reduced total (two-body plus three-body) potential, U^*_T, (Eqs. 24 and 26), and reduced quantum total potential (final potential), U^*_{QT}, (Eqs. 24, 26, 28). The size of time steps, Δt, and the number of time steps, n_t, and the cutoff radius, r_c, have been chosen as 0.01 ps, 50,000, and 3σ, respectively. The long-range correction terms have been evaluated using MOLDY to recover the contribution of the long-range cut-off of the intermolecular potential on the pressure and energy.

3.4.3 Thermodynamics properties

3.4.3.1 Pressure and internal energy We have performed MD simulation to obtain reduced pressure and internal energy of neon using our calculated reduced two-body potential which has been obtained using the inversion of viscosity data and the simple and accurate expression of

Wang and Sadus [18] for computing the three-body dispersion interactions. We have also included the quantum corrections, FH potential, for the potentials. The normal conventions have been adopted for the reduced density ($\rho^* = \rho\sigma^3$), reduced temperature ($T^* = kT/\varepsilon$), reduced internal energy ($E^* = E/\varepsilon$), and reduced pressure ($P^* = P\sigma^3/\varepsilon$) using the LJ parameters (Table 1).

Our results for reduced pressure and energy of neon in the NVT ensemble have been compared with the experimental [46] and previous theoretical works using MD simulations [20, 21, 25] at different temperatures and densities in Tables 4 and 5.

As Tables 4 and 5 show, there are better accordance between our simulated values of pressure and energy (especially the results from the final potential, U^*_{QT},) for neon and the experimental values than MD simulation of Eggenberger et al. [20] using an ab initio potential, Asger and Usmani [21] using Aziz HDFC2 potential and Leonhard and Deiters [25] using an ab initio potential with Axilrod-Teller three-body potential. Although this agreement is mainly due to our two-body potential for neon used in simulation, the pressure contribution from three-body potential of Marcelli and Sadus and the FH quantum potential has improved this agreement to some extent. It is also shown in these tables that the quantum corrections from the FH potential has great effect to the results than the three-body contribution of Wang and Sadus.

We have also studied the density and temperature effects on the pressure and energy results in Figs. 4 and 5, respectively. As these figures show, our simulated results using the final potential, U^*_{QT}, show better agreement with the experiment. This is due to the three-body contribution of Wang and Sadus [18] and the FH quantum potential that have improved the results and make them closer to the experiment. It is shown that these contributions have smaller effects on the energy results than the pressure values. As Fig. 5 shows, our simulated energy values are much smaller than the experiment which may be due to the fact that although FH potential improve the results but could not show full quantum behavior of neon atoms especially at lower temperatures when quantum effects become important [3].

As Figs. 4 and 5 show, the FH potential has great effects at lower temperatures. This makes sense because quantum effects become more significant at low temperatures. Although the three-body potential is more significant at higher densities, its role is much smaller than the quantum FH potential in improving the results.

3.4.3.2 Equation of state The MD results of the neon atoms have been used to determine the equation of state (EoS) for neon. We have calculated the reduced pressure of neon using the final potential, U^*_{QT}, for the reduced temperatures from 1.5 to 20 and reduced densities from 0.1 to 1.25 with the average precision about 4%. The careful investigation of the MD data indicates that the equation of state is:

$$P^* = a + bT^* + cT^{*2} \tag{29}$$

where a, b, and c obey the following equation:

Table 4 Comparison between our simulated results of reduced pressure of neon with the literature values at different temperatures and densities

T^*	ρ^*	P^*					
		Experiment [46]	Literature [20, 25]	Our work			
				P^*_2	P^*_{2Q}	P^*_T	P^*_{QT}
0.9146	0.0100	0.0086	0.0990	0.0086 ± 0.0001	0.0086 ± 0.0001	0.0085 ± 0.0002	0.0086 ± 0.0002
1.2195	0.0736	0.0643	0.6930	0.0604 ± 0.0057	0.0619 ± 0.0054	0.0594 ± 0.0044	0.0619 ± 0.0052
1.3415	0.1606	0.1160	1.2870	0.1000 ± 0.0173	0.1030 ± 0.0173	0.0980 ± 0.0168	0.1035 ± 0.0168
3.0488	0.3009	0.9896	1.0875	0.9256 ± 0.0653	0.9603 ± 0.0589	0.9257 ± 0.0658	0.9702 ± 0.0703
	0.6869	5.0411	5.8696	4.3758 ± 0.2564	4.9352 ± 0.2723	4.3907 ± 0.2544	4.9253 ± 0.2559
6.0976	0.1450	0.9898	1.0157	0.9751 ± 0.0349	0.9900 ± 0.0376	0.9752 ± 0.0347	0.9900 ± 0.0455
	0.4679	4.9550	5.3418	4.7322 ± 0.2044	4.9995 ± 0.2569	4.7322 ± 0.2272	4.9995 ± 0.2515
9.0854	0.2489	2.9494	3.0547	2.9007 ± 0.1104	2.9601 ± 0.1035	2.9057 ± 0.1233	2.9601 ± 0.1148
	1.0177	49.5000	54.5364	47.7180 ± 1.1138	51.9750 ± 0.9702	47.5200 ± 1.1385	51.975 ± 1.1880
12.1951	0.1967	2.9708	3.0414	2.9551 ± 0.0985	2.9898 ± 0.1040	2.9453 ± 0.0975	2.9948 ± 0.1282
	0.2907	4.9550	5.1281	4.9054 ± 0.1782	4.9995 ± 0.1836	4.8857 ± 0.2005	4.9995 ± 0.2237
15.2439	0.1632	2.9690	3.0227	2.9551 ± 0.0822	2.9849 ± 0.1094	2.9552 ± 0.1005	2.9799 ± 0.1079
	0.2455	4.9471	5.0760	4.9054 ± 0.1737	4.9995 ± 0.1688	4.9154 ± 0.1802	4.9995 ± 0.2336
18.2927	0.1395	2.9642	3.0094	2.9551 ± 0.0777	2.9849 ± 0.1267	2.9601 ± 0.0797	2.9898 ± 0.1084
	0.2126	4.9352	5.0427	4.9252 ± 0.2010	4.9995 ± 0.1634	4.9055 ± 0.2034	4.9995 ± 0.1515

Table 5 Comparison between our simulated results of reduced energy of neon with the literature values at different temperatures and densities

T^*	ρ^*	E^*					
		Experiment [46]	Literature [20, 21, 25]	Our work			
				E_2^*	E_{2Q}^*	E_T^*	E_{QT}^*
0.8320	0.8030	0.0191	−4.0551	−5.2688 ± 0.0257	−5.1126 ± 0.0367	−5.1569 ± 0.2935	−3.9812 ± 0.0330
0.9146	0.0100	5.6772	−0.1357	1.2763 ± 0.0183	1.2838 ± 0.0110	1.2722 ± 0.0110	1.2974 ± 0.0073
	0.7957	0.2567	−5.7450	−4.9992 ± 0.0367	−4.8499 ± 0.0367	−4.8818 ± 0.0367	−3.7328 ± 0.0367
1.0686	0.7468	0.8838	−4.1141	−4.2644 ± 0.0367	−4.1481 ± 0.0734	−4.1635 ± 0.0367	−3.0938 ± 0.2568
1.2195	0.0736	5.5788	−0.7337	1.0745 ± 0.0367	1.0795 ± 0.0367	1.0134 ± 0.0293	1.2345 ± 0.0293
	0.6157	2.0232	−8.1810	−3.0391 ± 0.0367	−2.8760 ± 0.0367	−2.9227 ± 0.0367	−2.0077 ± 0.0734
1.3415	0.1606	5.0828	−2.2012	0.5070 ± 0.0734	0.4984 ± 0.0367	0.4713 ± 0.0367	0.8609 ± 0.0367
	0.4684	3.1422	−2.8982	−1.7936 ± 0.0367	−1.6848 ± 0.0734	−1.7976 ± 0.0734	−0.9417 ± 0.0367
9.0854	0.2489	12.6934	13.2547	12.5437 ± 0.2935	12.5936 ± 0.2568	12.5462 ± 0.3302	12.8812 ± 0.1834
12.1951	0.1967	22.2541	18.0789	17.6118 ± 0.3302	17.6533 ± 0.4035	17.5990 ± 0.3302	17.8697 ± 0.5136
	0.2907	22.0696	18.2256	17.3462 ± 0.3669	17.4108 ± 0.3669	17.3279 ± 0.5503	17.7241 ± 0.2568

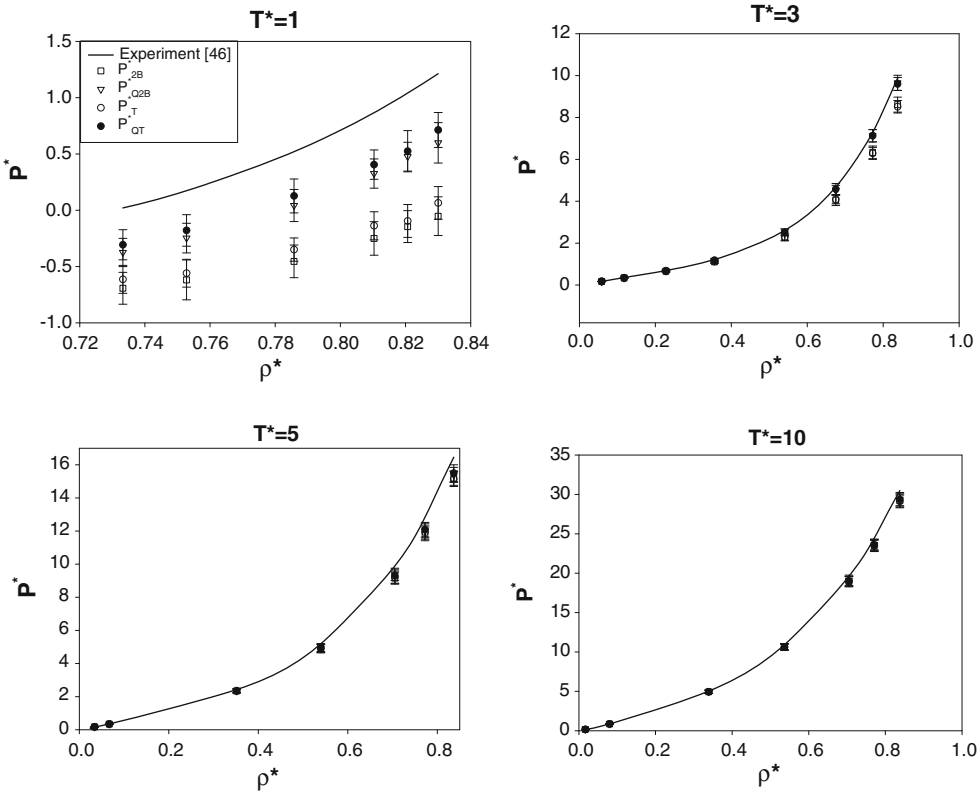

Fig. 4 Comparison between our simulated results of reduced pressure and experimental data at different reduced temperatures and densities using different potentials

$$X = \sum_{i=0}^{5} X_i \rho^{*i} \tag{30}$$

The values of the parameters of this equation have been given in Table 6.

We have compared our EoS with the experimental values [46] in Fig. 6 at different temperatures and densities. As Fig. 6 shows, our EoS is in a good agreement with the experiment but this agreement is smaller at higher densities.

3.4.4 Structural properties

Radial distribution function, $g(r)$, describes the structure of a liquid in terms of the probability of finding another particle at a given distance from a central particle relative to a uniform distribution of particles.

We have calculated radial distribution functions, $g(r)$, of neon at four state points using our calculated potentials and compared with the experimental values obtained using the

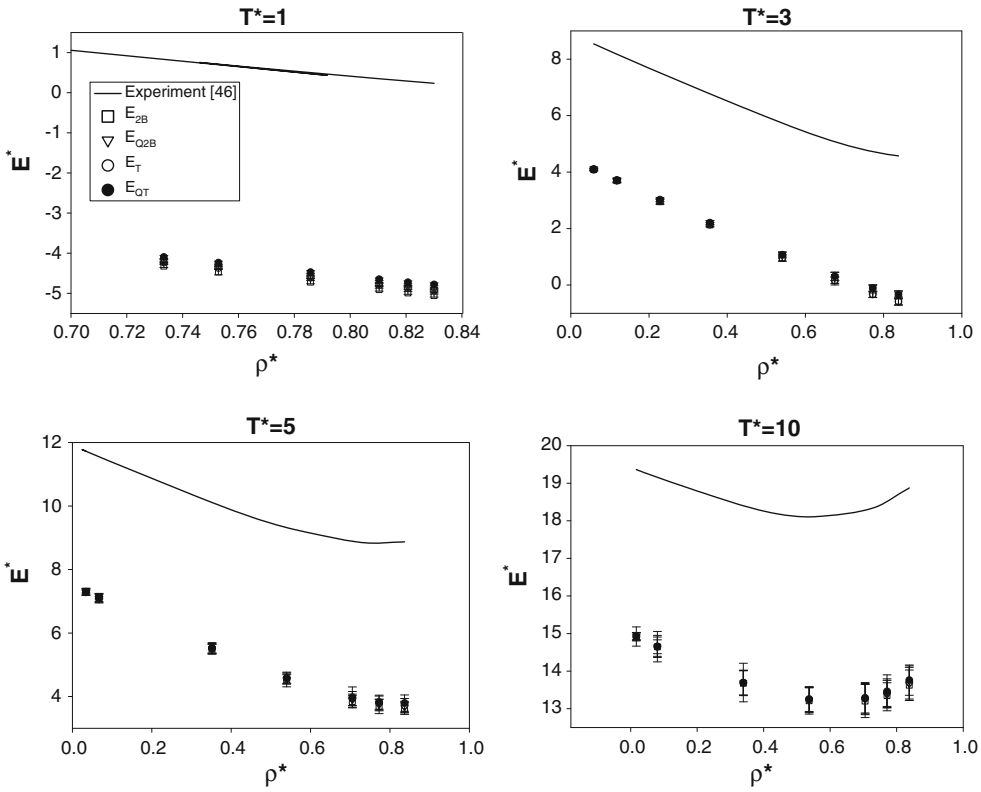

Fig. 5 Comparison between our simulated results of reduced energy and experimental data at different reduced temperatures and densities using different potentials

Table 6 Values of the coefficients of Eq. 30

X	X_o	X_1	X_2	X_3	X_4	X_5
a	−0.0315	2.0583	−22.3262	46.0241	−60.0788	38.0196
b	0.0067	0.5666	4.8892	−7.4129	11.1840	−4.1558
c	−0.0003	0.0165	−0.1389	0.3092	−0.3878	0.1426

neutron diffraction [47, 48] in Fig. 7. Figure 7 shows that the calculated $g(r)$ is in very good agreement with the experimental values that confirms the accuracy of the calculated potential. The different potentials give almost the same values of $g(r)$. This can be attributed to the fact that the quantum and three-body contribution do not affect the pair fluid structure strikingly [15].

Figure 7 shows that $g(r)$ becomes firstly zero at short distances, where repulsive forces prevent overlapping of particles. When r is close to the collision diameter, σ, (near the minimum of the potential curve) $g(r)$ increases rapidly to a maximum. As r increases gradually, $g(r)$ decreases showing that influence of the central molecule is disappearing and there is no order at long distances.

3.4.5 Transport properties

3.4.5.1 Self-diffusion coefficient The self-diffusion coefficient, D, can be calculated from the time-dependent mean-square displacement of particles, according to the Einstein formula [49] that is expected linear at long times:

$$D = \lim_{t\to\infty} \frac{1}{6tN} \sum_{i=1,N} \left\langle |r_i(t) - r_i(0)|^2 \right\rangle \tag{31}$$

where $r_i(0)$ and $r_i(t)$ are the positions of the particles at time $t = 0$ and t, respectively.

We have compared our calculated reduced self-diffusion coefficient of neon from calculated using the Einstein formula with the experimental values for different densities at $T^* = 1.13$ [50] (Fig. 8). As this figure shows, our calculated reduced self-diffusion coefficients are in good agreement with the experimental values. Similar to our results for the thermodynamic properties, it is clear that the quantum corrections from the FH potential have greater effects on the self-diffusion values than those of the three-body corrections of Wang and Sadus.

3.4.5.2 Shear viscosity The shear viscosity of a liquid is related to the fluctuations of the off-diagonal elements of the pressure or stress tensor. The viscosity can be calculated from an equilibrium simulation by integrating the Green–Kubo (GK) formula [49]:

$$\eta = \frac{V}{3kT} \int_0^\infty \left\langle \sum_{x<y} P_{xy}(t) P_{xy}(0) \right\rangle dt \tag{32}$$

where η is the shear viscosity, V is the system volume, and P_{xy} refers to the xy component of the stress. The brackets

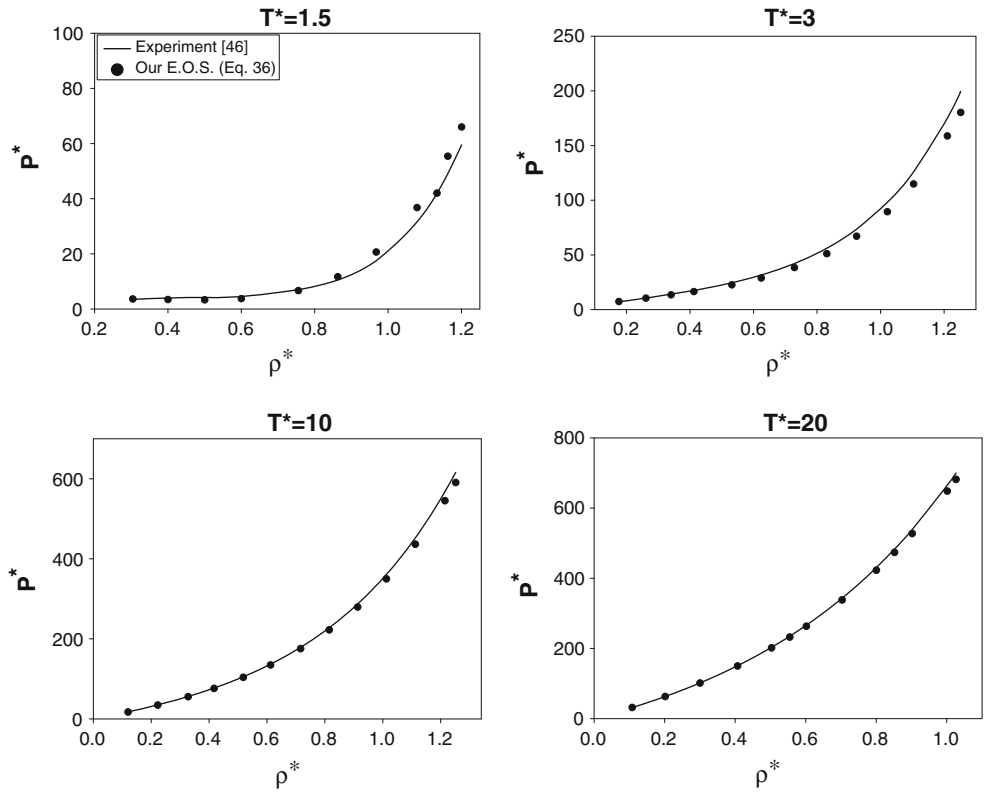

Fig. 6 Comparison between our equation of state and experimental data at different reduced temperatures and densities

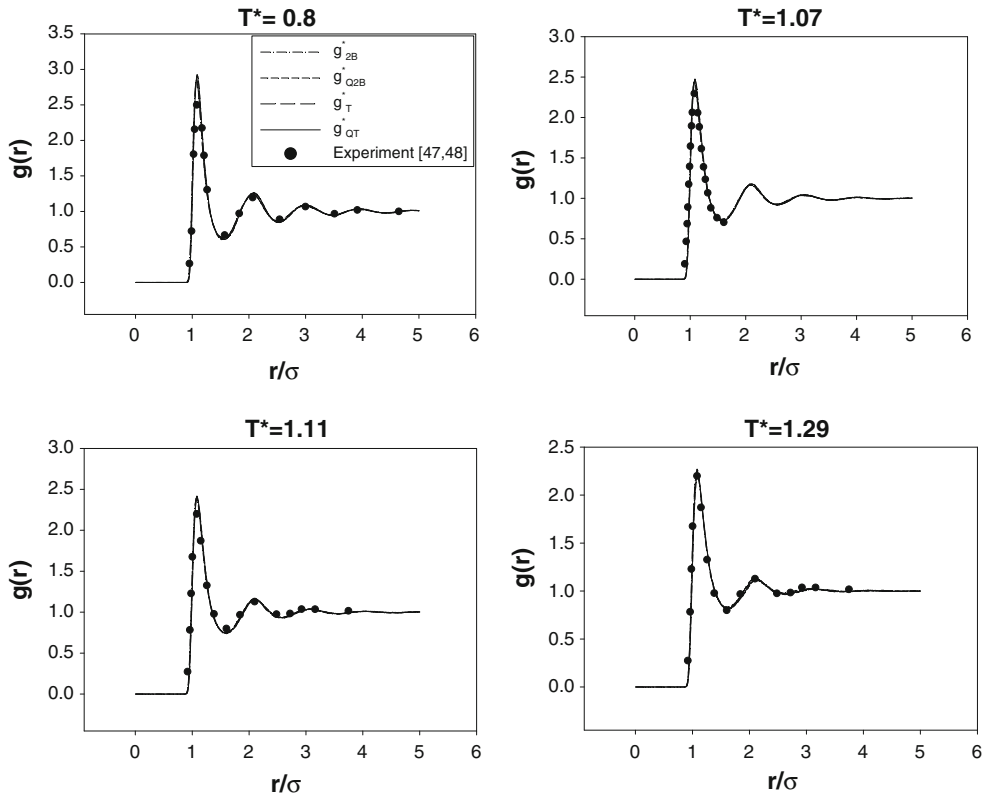

Fig. 7 Comparison between our simulated results and experimental data of radial distribution function at four reduced temperatures using different potentials

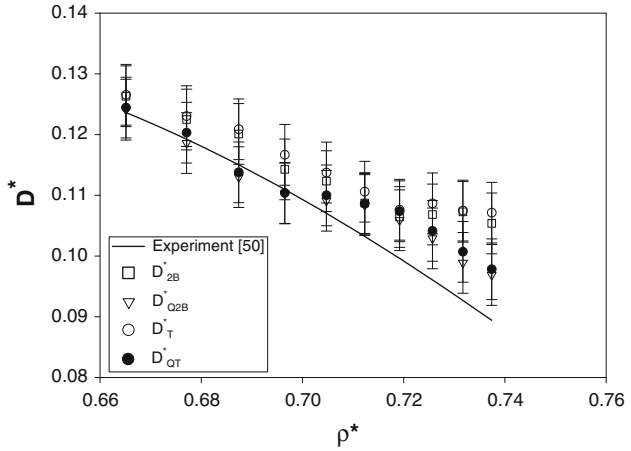

Fig. 8 Comparison between our simulated results and experimental data of self-diffusion coefficient at $T^* = 1.13$ using different potentials

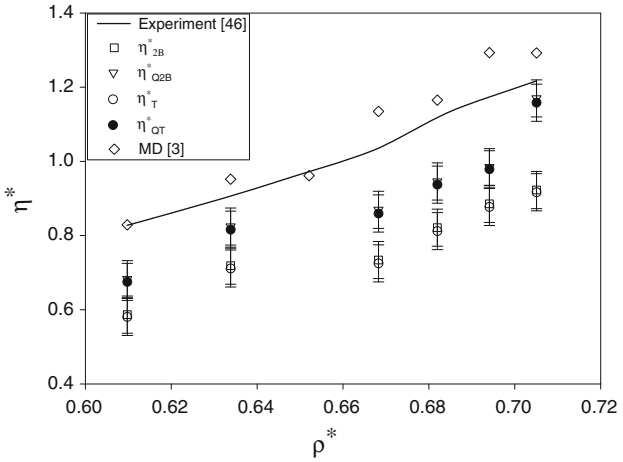

Fig. 9 Comparison between our simulated results and literature values of shear viscosity at $T^* = 1.37$ using different potentials

indicate an averaging over time origins. The component of the microscopic stress tensor is given by:

$$P_{xy}(t) = \sum_{i=1}^{N} \left(m v_i^x v_i^y - \frac{1}{2} \sum_{i \neq j} \frac{r_{ij}^x r_{ij}^y \partial V_{ij}}{r_{ij} \ \partial r_{ij}} \right) \tag{33}$$

where υ_i are the velocities of particles at time t, and V_{ij} is the interaction potential of the system.

The GK formulation utilizes a single summation that consolidates the contributions of all the atoms into a single autocorrelation function thereby allowing the formulation to be used with the molecular dynamics simulations.

The stress autocorrelation function necessarily involves the entire system. Consequently, we cannot improve the statistical precision of results for viscosity by averaging over the N particles in the system. However, the statistical precision can be improved fairly by averaging over all three terms that result from the stress tensor:

$$\eta = \frac{1}{3} \left(\eta_{xy} + \eta_{yz} + \eta_{zx} \right) \tag{34}$$

We have compared our simulated reduced shear viscosity coefficient of neon at $T^* = 1.37$ for different densities using our calculated potentials with the experimental [46] and the MD values of Tchouar et al. [3] in Fig. 9. As this figure shows, although our calculated reduced viscosities are in fairly good agreement with the experiment, they are smaller than the experimental values compared with the MD values of Tchouar et al. [3] that are bigger than the experiment. Again, the quantum contribution from the FH potential has superior effect on the viscosity than the three-body contribution of Wang and Sadus.

4 Conclusions

We have determined the pair potential energy function of neon via the inversion of reduced viscosity collision integrals at zero pressure and fitted with a HFD-like potential. This potential can reproduce the second virial coefficient, viscosity, thermal conductivity, and self-diffusion coefficient of neon in a good accord with the experimental data over wide ranges of temperatures and densities.

We have also performed molecular dynamics simulation to obtain pressure, internal energy, radial distribution function, self-diffusion coefficient, and shear viscosity of fluid neon at different temperatures and densities using our calculated pair potential supplemented by quantum corrections following the Feynman–Hibbs approach. The significance of this work is that the three-body expression of Wang and Sadus [18] can be used to improve the prediction of the pressures of neon without requiring an expensive three-body calculation. The molecular dynamics simulation of neon has been also used to determine a new equation of state for neon. Our results show that the quantum contribution from the FH potential has superior effect on the calculated properties than the three-body formula of Wang and Sadus.

Acknowledgments The authors would like to express their sincere thanks to Mr. F. Behnia for helpful guidance for running the simulation program in Linux system in self-diffusion coefficient calculation.

References

1. Maitland GC, Rigby M, Smith EB, Wakeham WA (1987) Intermolecular forces, their origin and determination. Clarendon Press, Oxford
2. Goharshadi EK (1998) Int J Thermophys 19:227–237

3. Tchouar N, Ould-Kaddour F, Levesque D (2004) J Chem Phys 121:7326–7331
4. Tchouar N, Benyettou M, Ould-Kaddour F (2005) J Mol Liq 122:69–73
5. Wigner EP (1932) Phys Rev 40:749–759
6. Kirkwood JG (1933) Phys Rev 44:31–37
7. Hansen JP, Weis JJ (1969) Phys Rev 188:314–318
8. Feynman RP, Hibbs A (1965) Quantum mechanics and path-integral. McGraw-Hill, New York
9. Sese LM (1991) Mol Phys 74:177–189
10. Sese LM (1993) Mol Phys 78:1167–1177
11. Goharshadi EK, Abbaspour M, Kashani H, Baherololoom M (2008) Theor Chem Account 119:355–368
12. Barker JA, Fisher RA, Watts RO (1971) Mol Phys 21:657–673
13. Monson A, Rigby M, Steele WA (1983) Mol Phys 49:893–898
14. Elrod MJ, Saykally RJ (1994) Chem Rev 94:1975–1997
15. Marcelli G, Todd BD, Sadus RJ (2001) J Chem Phys 115:9410–9413
16. Marcelli G, Sadus RJ (1999) J Chem Phys 111:1533–1540
17. Axilrod BM, Teller E (1943) J Chem Phys 11:299–300
18. Wang L, Sadus RJ (2006) J Chem Phys 125:144509–1–144509–5
19. Goharshadi EK, Abbaspour M (2006) J Chem Theory Comput 2:920–926
20. Eggenberger R, Gerber S, Huber H, Searles D, Welker M (1993) J Chem Phys 99:9163–9169
21. Asger M, Usmani QN (1999) Physica B 271:104–115
22. Vogt PS, Liapine R, Kirchner B, Dyson AJ, Huber H, Marcellib G, Sadus RJ (2001) Phys Chem Chem Phys 3:1297–1302
23. Tchouar N, Benyettou M, Ould-Kaddour F (2003) Int J Mol Sci 4:595–606
24. Nasrabad AE, Laghaei R, Deiters UK (2004) J Chem Phys 121:6423
25. Leonhard K, Deiters UK (2000) Mol Phys 98:1603–1616
26. Chapman S, Cowling TG (1970) Mathematical theory of non-uniform gases. Cambridge University Press, New York
27. Bzwoski J, Kestin J, Mason EA, Uribe FJ (1990) J Phys Chem Ref Data 19:1179–1232
28. Boushehri A, Bzowski J, Kestinand J, Mason EA (1987) J Phys Chem Ref Data 16:445–466
29. Goharshadi EK, Abbaspour M, Morsali A (2003) Ind Eng Chem Res 42:2256–2261
30. Najafi B, Mason EA, Kestin J (1983) Physica A 119:387–440
31. Clancy P, Cough DW, Matthews GP, Smith EB, Maitland GC (1975) Mol Phys 30:1397–1407
32. Aziz RA, Meath WJ, Allnet AR (1983) Chem Phys 78:295–309
33. Assael MJ, Trusler JPM, Tsolakis TF (1996) Thermophysical properties of fluids. Imperial College Press, London
34. Dymond JH, Smith EB (1980) The virial coefficients of pure gases and mixtures. Oxford University Press, New York
35. Rainwater JC (1984) J Chem Phys 81:495–510
36. Friend DG, Rainwater JC (1984) Chem Phys Lett 107:590–594
37. Najafi B, Ghayeb Y, Parsafar G (2000) Int J Thermophys 21:1011–1031
38. Bich E, Millat J, Vogel E (1990) Phys Chem Ref Data 19:1289–1305
39. Dawe RA, Smith EB (1970) J Chem Phys 52:693–703
40. Kestin J, Paul R, Clifford AA, Wakeham WA (1980) Physica A 100:349–369
41. Saxena VK, Saxena SC (1968) J Chem Phys 56:5662–5667
42. Hirschfelder JO, Curtis CF, Bird RB (1954) Molecular theory of gases and liquids. Willy, New York
43. Winn EB (1950) Phys Rev 80:1024–1027
44. Smit B, Hauschild T, Prausnitz M (1992) Mol Phys 77:1021–1031
45. The MOLDY program was coded by Refson K, and can be downloaded from the internet at http://wwwearthoxacuk/%7Ekeith/moldyhtml
46. NIST chemistry webbook. Available at http://webbook.nist.gov/chemistry/fluid
47. deGraaf LA, Mozer B (1971) J Chem Phys 55:4967–4973
48. Bellissent-Funel MC, Buontempo U, Filabozzi A, Petrillo C, Ricci FP (1992) Phys Rev B 45:4605–4613
49. Allen M, Tildesley D (1987) In computer simulation of liquids. Oxford University Press, Oxford
50. Bewilogua L, Gladun C, Kubsch B (1971) Low Temp Phys 4:299–303